Leaf and Plant Age Affects Photosynthetic Performance and Photoprotective Capacity[1]

Ludwik W. Bielczynski,[a,2] Mateusz K. Łącki,[b] Iris Hoefnagels,[a] Anna Gambin,[b] and Roberta Croce[a]

[a]Biophysics of Photosynthesis/Energy, Faculty of Sciences, Department of Physics and Astronomy, VU Amsterdam, 1081 HV Amsterdam, The Netherlands

[b]Institute of Informatics, University of Warsaw, 02-097 Warsaw, Poland

ORCID IDs: 0000-0002-0831-4536 (L.W.B.); 0000-0001-7415-4748 (M.K.Ł.); 0000-0003-3476-3017 (A.G.); 0000-0003-3469-834X (R.C.).

In this work, we studied the changes in high-light tolerance and photosynthetic activity in leaves of the Arabidopsis (*Arabidopsis thaliana*) rosette throughout the vegetative stage of growth. We implemented an image-analysis work flow to analyze the capacity of both the whole plant and individual leaves to cope with excess excitation energy by following the changes in absorbed light energy partitioning. The data show that leaf and plant age are both important factors influencing the fate of excitation energy. During the dark-to-light transition, the age of the plant affects mostly steady-state levels of photochemical and nonphotochemical quenching, leading to an increased photosynthetic performance of its leaves. The age of the leaf affects the induction kinetics of nonphotochemical quenching. These observations were confirmed using model selection procedures. We further investigated how different leaves on a rosette acclimate to high light and show that younger leaves are less prone to photoinhibition than older leaves. Our results stress that both plant and leaf age should be taken into consideration during the quantification of photosynthetic and photoprotective traits to produce repeatable and reliable results.

Heterogeneity in photosynthetic capacity among leaves in an individual plant has been largely reported in plant species that form part of a canopy. As a consequence of the light gradient between overlapping leaf layers (*Solidago altissima*; Hirose and Werger, 1987a, 1987b) or regardless of canopy (*Ipomea tricolor*; Hikosaka et al., 1994), the photosynthetic rates and nitrogen use efficiency decline with leaf age. It was suggested recently that individual leaves in the rosette of the model plant Arabidopsis (*Arabidopsis thaliana*) respond differently to abiotic stresses (Bresson et al., 2015; Flood et al., 2016); however, the heterogeneity of photosynthesis among leaves of the same plant has been partially addressed (Wingler et al., 2004) but not fully assessed.

Depending on the age of the plant, the emerging leaves of Arabidopsis differ in shape, and the cells composing them differ in thickness and size (Kerstetter and Poethig, 1998; Tsukaya, 2013). Leaf anatomy influences the photosynthetic capacity, such as by changing the mesophyll thickness and increasing the space for chloroplasts at the cell surface necessary for the gas exchange (Oguchi et al., 2003). Thus, it can be expected that structural differences in Arabidopsis leaves could be at least partially responsible for heterogeneity in photosynthesis in the leaves of a rosette.

Additionally, the leaves on an Arabidopsis rosette are always of different age. In several plant species, such as rice (*Oryza sativa*; Makino et al., 1983), soybean (*Glycine max*; Jiang et al., 1993), and tobacco (*Nicotiana tabacum*; Jiang and Rodermel, 1995; Miller et al., 1997, 2000), an initial increase in the photosynthetic rate during leaf expansion is followed by a decrease upon maturation and a sharp drop during senescence due to major changes in the photosynthetic apparatus (Ghosh et al., 2001; Wada et al., 2009; Brouwer et al., 2012; Mohapatra et al., 2013; Mulisch and Krupinska, 2013; Nath et al., 2013). However, in Arabidopsis, it was shown that, during whole-leaf development, the photosynthetic rate per fresh weight decreases gradually (Stessman et al., 2002).

Additionally, the photosynthetic activity of Arabidopsis changes during the vegetative stage, and as the plant gets older, its tolerance to high light (HL) increases (Carvalho et al., 2015). Based on these reports, we hypothesized that photosynthetic heterogeneity should exist among leaves of a single plant and that both photosynthetic performance and photoprotective capacity will be influenced by the time of emergence, the age of the leaf, and the age of the plant itself.

Arabidopsis is a particularly interesting case for several reasons. (1) It is a model plant popular in studies where accurate phenotyping of photosynthesis-related traits is crucial. (2) Its leaves are only moderately

[1] L.W.B. and R.C. were supported by the BioSolar Cells research program, sponsored by the Dutch Ministry of Economic Affairs and by the European Research Council (ERC consolidator ASAP to R.C.); M.K.Ł. and A.G. were supported by the Polish National Science Center grants 2015/17/N/ST6/03565 and 2012/06/M/ST6/00438 (to A.G.).

[2] Address correspondence to l.w.bielczynski@vu.nl.

The author responsible for distribution of materials integral to the findings presented in this article in accordance with the policy described in the Instructions for Authors (www.plantphysiol.org) is: Ludwik W. Bielczynski (l.w.bielczynski@vu.nl).

www.plantphysiol.org/cgi/doi/10.1104/pp.17.00904

heterobaric (Cheeseman, 1991; Terashima, 1992), meaning that the histology in a different part of the leaf causing nonuniform gas exchange will only slightly influence the photosynthetic performance at the level of a single leaf (Morison and Lawson, 2007). (3) Due to the rosette architecture, for the major part of leaf development, a light gradient due to shading of the upper leaves is absent.

During the light-dependent phase of photosynthesis, light absorption by PSII and PSI is used to create reducing power (NADPH) and ATP, which are then used in the Calvin-Benson cycle for CO_2 assimilation. Cytochrome b_6f acts as an intermediate for the linear electron flow (LEF) between PSII and PSI and enhances the proton gradient across the thylakoid membrane (ΔpH). However, as plants grow in variable light conditions, they are often subjected to suboptimal light conditions. The rate of the LEF can be adjusted accordingly by the following mechanisms. (1) The aperture of stomata can increase to facilitate gas exchange and increase the availability of CO_2 for assimilation under HL (Mott, 2009). (2) Regulation of Rubisco activation can tune the rate of carbon fixation to the rate of LEF (Spreitzer and Salvucci, 2002; Carmo-Silva and Salvucci, 2013). (3) LEF through the cytochrome b_6f complex can decrease as the lumen becomes more acidic, which signals overexcitation (Schöttler et al., 2015).

When the photon flux exceeds the photosynthetic capacity, it can damage the photosynthetic apparatus. To avoid photodamage, plants have evolved several photoprotective mechanisms. Those that are activated within seconds/minutes are collectively called nonphotochemical quenching (NPQ), as their main role is to quench the excess of excitation energy. There are three major components of NPQ; however, under HL illumination, only two of them play a role. (1) As the ΔpH builds up across the thylakoid membrane, it triggers energy dissipation through heat by the concerted action of the protein PsbS (Li et al., 2000) and the xanthophyll cycle (Demmig-Adams, 1990) via a process that is not fully understood. (2) Controlled damage and inactivation of the PSII reaction center, or photoinhibition (Quick and Stitt, 1989), reduces the incoming light energy and prevents downstream damage to PSI. Damaged PSII reaction centers are later replaced in the PSII repair cycle (Aro et al., 2005).

The photosynthetic and photoprotective capacity of photosynthetic organisms often is studied using pulse amplitude-modulated (PAM) fluorometry. In the case of standard fiber-optic PAM fluorometers, the measurement is usually performed on a selected spot of an individual leaf of a few different plants, or in the case of imaging setups, by averaging the signal from whole plants. To study in more detail the spatially resolved photosynthetic and photoprotective capacity of a plant throughout the vegetative stage, we used an imaging setup to follow the changes in energy partitioning (i.e. the distribution of the absorbed energy by PSII between different deexcitation pathways). The idea of energy partitioning is based on the general concept introduced by Genty et al. (1996) and described by Cailly et al. (1996). In short, the absorbed energy can be (1) used for photochemical conversion to drive photosynthesis; (2) dissipated by regulated thermal energy dissipation (NPQ); (3) radiated as nonregulated heat dissipation; (4) emitted as fluorescence; or (5) used for other processes. Several ways to measure and calculate energy partitioning have been proposed (Lazár, 2015); here, due to its simplified formulation and correspondence with other methods, we utilize the method of Klughammer and Schreiber (2008).

An arbitrary distinction between short-term responses and long-term acclimation to HL conditions is often made (Kono and Terashima, 2014). It is assumed that short-term responses (which include NPQ) occur in a range from seconds to minutes (Tikhonov, 2015) and involve the rearrangement of existing chloroplast components. During long-term acclimation (from hours to weeks), changes occur in the architecture of the anatomy of the plant (Sims and Pearcy, 1992), and in the pigment and protein composition of the photosystems (Ballottari et al., 2007), due to the selective synthesis and degradation of various components. To cover both scenarios, we tested both the short- and long-term responses of Arabidopsis leaves at different ages to HL.

The aim of this study was to investigate the changes in energy partitioning during growth throughout the vegetative stage. We first performed the study on the whole-plant level for multiple plants to establish the extent of changes due to the phenotypic variation and the plant's age. Then, we proceeded with a systematic study of energy partitioning within the leaves of a rosette. During exploratory data analysis, we formulated the hypothesis that heterogeneity in energy partitioning between the leaves was due to the combined effect of leaf and plant age. This was then verified using a customized statistical work flow based on Dirichlet regression. We show that both leaf and plant age are important parameters in assessing photosynthetic performance and photoprotective capacity. Furthermore, we investigated the acclimation capacity of different leaves in the rosette to long HL exposure (8 d long). We finished our investigation by validating the effect of the light intensity on energy partitioning.

RESULTS

Whole-Plant Level

Heterogeneity in Energy Partitioning

In order to investigate if the photosynthetic activity is homogenous throughout the whole plant, we imaged the fluorescence of chlorophyll *a* during quenching analysis (an exemplary raw fluorescence trace is shown in Supplemental Fig. S2). We calculated quantum yields of photochemical conversion (Φ_{PSII}) and regulated thermal energy dissipation (Φ_{NPQ}), and we summed together fluorescence, nonregulated heat dissipation, and other processes (Φ_{NO}). This method has the advantage that only

measurements of transient fluorescence (F_t) and maximal fluorescence in dark- (F_M) and light-acclimated (F_M') states are needed to calculate the above-mentioned quantum yields. These terms do not depend on measurements of minimal fluorescence in dark- (F_0) and light-acclimated (F_0') states, which are troublesome and usually inaccurate, especially in imaging setups (lower signal-to-noise ratio than in traditional setups) due to the contribution from PSI (Pfündel et al., 2013).

The parameters related to the energy partitioning in PSII were followed until they reached a steady-state level (Fig. 1). Performing a full quenching analysis made it possible to observe the kinetics of NPQ activation instead of just the final level at a given actinic light (AL) intensity. In our experiments, to ensure NPQ activation and to induce as little photodamage as possible, we used AL of 500 μmol photons m^{-2} s^{-1}, which was almost 3 times the growth light intensity.

It was suggested that, under HL illumination, high values of Φ_{NPQ} indicate increased photoprotective capacity (Klughammer and Schreiber, 2008). In those conditions, the response of the photosynthetic apparatus is aimed for a maximal Φ_{PSII}, a minimal Φ_{NPQ} and Φ_{NO}, and a maximal Φ_{NPQ}/Φ_{NO} ratio. A low Φ_{NPQ}/Φ_{NO} ratio leads to photodamage. Note that the Φ_{NPQ} and Φ_{NO} parameters can be estimated only when the rate constants of nonregulated heat dissipation and fluorescence remain constant while measuring F_t and F_M. If during the time-dependent measurement (dark-to-light transition) the illumination is photoinhibitory, then an increase in the rate constant of nonregulated heat dissipation will be erroneously interpreted as an increase in Φ_{NPQ}. However, during short measurements when AL is high-intensity, nonphotoinhibitory red light, Φ_{NPQ} will represent the fraction of energy quenched in the energy dissipation through heat.

The initial assessment was performed by a visual study of the chosen parameters mapped on the image of a rosette (Fig. 1). At each saturating pulse (SP) during light acclimation (referred to below as pulse), the distribution of Φ_{PSII} was relatively homogenous (Fig. 1A). In contrast, leaves on the rosette differed mostly in the levels of Φ_{NPQ} and Φ_{NO} (Fig. 1, B and C), especially during the initial period of the dark-to-light transition (i.e. during NPQ activation [for details, see "Statistical Analysis"]).

To summarize the plant-wise distribution of the three quantum yields Φ_{PSII}, Φ_{NPQ}, and Φ_{NO}, we treated each pixel in Figure 1, A to C, as a point of a triangle where the point coordinates sum to 1 (Fig. 1D). Previously, the aim of several studies was to understand the regulation of photosynthesis and photoprotection under various environmental conditions (Demmig-Adams et al., 1996; Hendrickson et al., 2004; Kramer et al., 2004; Schreiber and Klughammer, 2008; Klughammer and Schreiber, 2008; Martínez-Peñalver et al., 2012). As a consequence, the major focus was on the central values of energy partitioning, and very little attention was given to the variation and distribution. We introduce a more intuitive way to describe energy partitioning during well-known phenomena (i.e. photosynthetic activation and NPQ induction) that also broadens our view of the distributions of these values during the quenching analysis.

Here, we describe only the first, second, third, and seventh pulses. These are representative of the full range of states of the photosynthetic apparatus, as changes in energy partitioning become less distinct during the convergence to the steady-state level.

During the first pulse, when the carbon cycle enzymes and the ΔpH-dependent NPQ are not activated, we observed a high Φ_{NO} (around 80%), with Φ_{NPQ} close to zero and Φ_{PSII} around 20%. The distribution of the three parameters was approximately unimodal and narrow. In the second pulse, Φ_{PSII} did not change, but the activation of the regulated NPQ resulted in an increase of Φ_{NPQ} (to around 40%) and a proportional decrease in levels of Φ_{NO}. A considerable amount of variance was observed in the levels of Φ_{NPQ} and Φ_{NO}. The results (Fig. 1B) suggests that leaves located at the center of the rosette activate NPQ sooner than those at the edge. During the third pulse, the Φ_{PSII} shifted to slightly higher values (around 30%). The distribution of Φ_{NPQ} and Φ_{NO} became slightly less dispersed, and while the values of the former remained around 40%, those of the latter decreased to around 30%. Throughout the remaining series of pulses, we observed an increase in the amount of energy used for photochemistry and a decrease in both NPQ parameters. Finally, after the seventh pulse, the system reached 40% Φ_{PSII} and 30% for both Φ_{NPQ} and Φ_{NO}, which should well approximate the steady-state level. The parameters followed a unimodal distribution, narrower for Φ_{PSII} and Φ_{NO} than for Φ_{NPQ}.

At the onset of the dark-to-light transition, the distributions of parameters related to dissipation of the excess of excitation energy (Φ_{NPQ} and Φ_{NO}) are broader, suggesting a spatial heterogeneity of response.

The leaves on the rosette activated NPQ at different rates. This suggests a range of photoprotective responses during light intensity fluctuations. As the Φ_{PSII} reaches steady state, it is proportional to the assimilation rate (Genty et al., 1989). At that time, the narrowed distribution of Φ_{NO} values compared with those of Φ_{PSII} can be interpreted as performance tuning rather than an enhanced photoprotection of the photosynthetic apparatus.

Phenotypic Variation

Since only a homozygous wild-type line was studied, the phenotypic variation was expected to be minimal and mostly due to small fluctuations in the plant's growth conditions (Fig. 2). To investigate the variation in energy partitioning among the wild-type plants, we analyzed 20 different plants at a specific time point (day 23 of growth; Fig. 2A). Ternary plots (Fig. 2B) suggest very small variations in the values and dispersion of the energy partitioning between different plants. During the second pulse of the quenching analysis, the highest

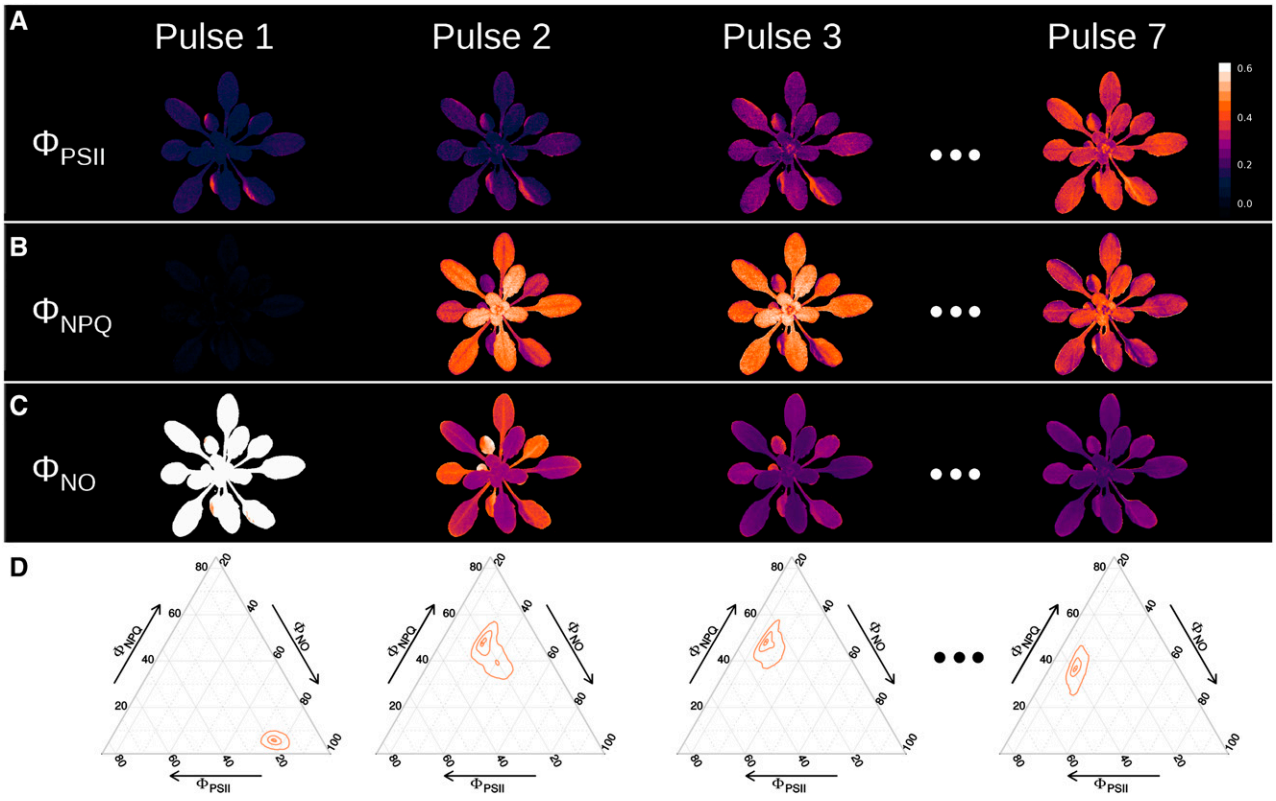

Figure 1. Imaging of the energy distribution on the rosette during a dark-to-light transition. A to C, Changes in values and spatial distribution of Φ_{PSII}, Φ_{NPQ}, and Φ_{NO} (A, B, and C, respectively) during the first, second, third, and seventh pulses (left to right columns, respectively) on a 3-week-old plant. The values from 0 to 0.6 are mapped as a color gradient (from dark violet to light yellow). The color scale is shown on the right side in A. D, Ternary plots display the distribution of energy between Φ_{PSII}, Φ_{NPQ}, and Φ_{NO}. The axes correspond to the fractions of Φ_{PSII} (bottom axis), Φ_{NPQ} (left axis), and Φ_{NO} (right axis). The contours represent estimates of borders of regions encompassing 99.73%, 95.45%, 68.75%, and 20% of sample points.

variance between the replicates was observed in Φ_{NO} and Φ_{NPQ} (Fig. 2B). As the chlorophyll fluorescence reached steady state, the situation was reversed and the largest variance was observed in Φ_{NPQ} and Φ_{PSII}, while the distribution of Φ_{NO} was narrow. The differences between plants were relatively small, and they all followed the patterns of the plant described above.

Changes during Growth

To observe the full extent of changes in energy partitioning during growth, we performed quenching analysis every other day during 32 d of growth (Fig. 3). During a standard quenching analysis, measurements are performed on selected leaves of similar age or over the whole exposed area of a plant by averaging the collected information. To investigate general trends, we followed the latter approach, averaging out information over the whole exposed area of three different plants (Fig. 3A).

Close to pulse 7, we observed an increase in the values of Φ_{PSII} (approximately from 22% to 41%) and a decrease in the values of Φ_{NPQ} (approximately from 55% to 30%) when the plants get older. During the whole vegetative growth, differences in energy partitioning between the leaves of the same plant (Fig. 3B) followed patterns observed during the one time-point analysis (Fig. 1). Large variance and a broadened distribution in the Φ_{NO} and Φ_{NPQ} during the second pulse were conserved over time (Fig. 3C), while the spread of Φ_{PSII} and Φ_{NPQ} became smaller when reaching steady state.

The changes in the distributions might be related to the contributions from leaves of different ages. When the plants are young, the signal originates only from young leaves. At later time points, the growth of leaves complicates the overall picture, as each new leaf grows a limited amount of time and subsequent leaves usually grow larger than the previous ones. As a consequence, older rosettes are composed of leaves of different ages and variable size. The largest light interception area is spanned by middle-aged, fully expanded leaves that tend to cover older ones. Analyzing the averaged signal restricts the analysis to this dominant group of leaves. To get a better understanding of the diversity of the signal source, we investigated in more detail the energy partitioning at the subrosette level.

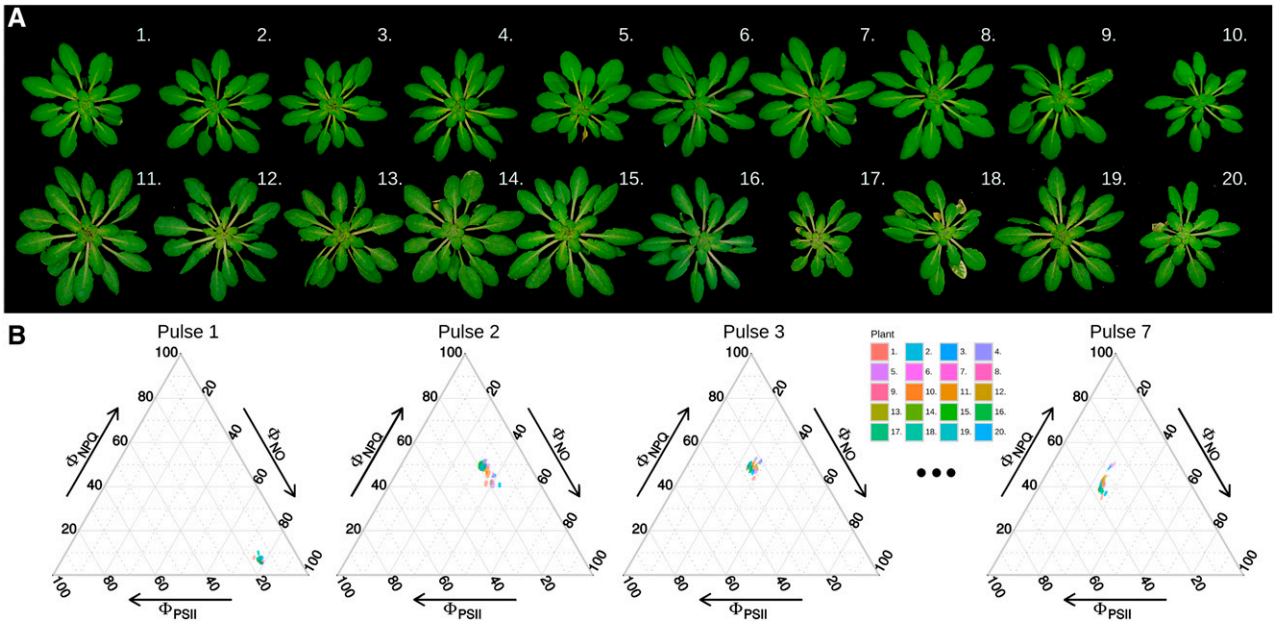

Figure 2. Phenotypic variation during Arabidopsis growth. A, Twenty plants from the same hydroponic setup measured on the same day. B, Ternary plots of the same plants (color-coded density contours) during pulses 1, 2, 3, and 7 of the quenching analysis. Colored regions contain 99.73% of observations gathered on one plant.

Subrosette Level

Energy Partitioning and Leaf Number

It was observed that leaves differ in their response to the dark-to-light transition. To study this in detail, we performed a semiautomated disassembly of the fluorescence images of the rosettes. The same leaves were traced on different images and ordered based on their emergence times (Supplemental Fig. S3). Energy partitions depend heavily upon this ordering (Fig. 4A) but not on spatial positioning due to complicated leaf growth dynamics, as mentioned before. To investigate this point, we studied the relationship of energy partitioning and the leaf number (Fig. 4B).

Two distinct behaviors are discernible. At the second pulse, younger leaves (higher leaf number) show higher values of Φ_{NPQ} and lower Φ_{NO}, while Φ_{PSII} remained similar for different leaves. The largest NPQ-related differences between leaves were always observed during the second pulse of the quenching analysis, indicating larger variation in the activation time of the quenching processes. However, upon reaching the steady state, the differences between older and younger leaves became less pronounced and the trend changed: younger leaves had reduced levels of Φ_{NPQ} and increased levels of Φ_{PSII}. The Φ_{NO} decreased slightly with the leaf number.

Changes Due to Leaf Age

We hypothesized that the differences in energy partitioning observed between the leaves of a rosette were mostly due to the different ages of the leaves. Thus, we investigated how the photosynthetic activity changes during the growth of a leaf (Fig. 5A). We recorded the moment of appearance of each leaf and calculated its age in days. As observed previously for the leaf number, the changes were largest at the beginning of the quenching analysis (second pulse). When the leaves were maturing, the level of Φ_{NPQ} dropped and that of Φ_{NO} increased (Fig. 5B). Both parameters changed in a slightly sigmoidal manner. The Φ_{PSII} rose gradually with the age of the leaves. At the steady-state time point, changes were similar but less pronounced.

Combined Responses of the Age of the Plant and Its Leaves on the Energy Partitions

To study the combined effects of the age of the plant and its leaves on energy partitioning, we prepared a plot that maps each observed pair (plant age and leaf age) to a color encoding the fraction of energy corresponding to a given quantum yield (Fig. 6). Two different responses were observed: (1) during the second pulse, the values change mostly with leaf age (i.e. along the y axis), whereas (2) in the seventh pulse, changes depend mostly on plant age, showing variation along the x axis. For response 1, the largest changes were observed in Φ_{NPQ}, which decreased with the age of the leaf. An inverse relationship was observed with the other two parameters (to a smaller extent for Φ_{PSII}), as their values increased with the age of the leaf. In the case of response 2, Φ_{PSII} increased with plant age, Φ_{NPQ} decreased, and Φ_{NO} remained stable.

In summary, the results indicate that both the age of the leaf and the age of the plant influence the photosynthetic

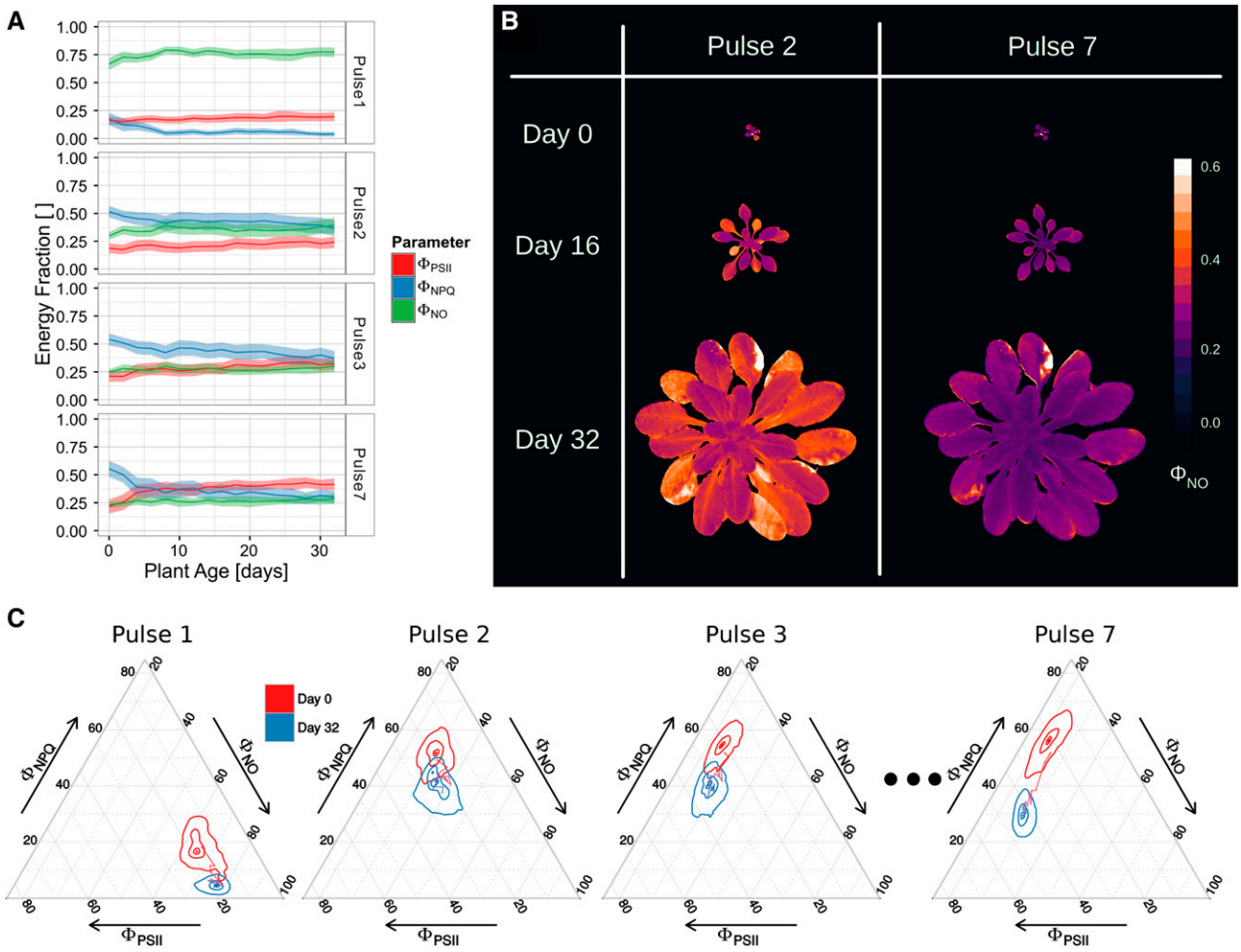

Figure 3. Changes in energy distribution in the photosynthetic apparatus during 32 d of growth. A, Changes in Φ_{PSII}, Φ_{NPQ}, and Φ_{NO} during plant growth (red, blue, and green traces and shadows, respectively). Only a selection of SPs (pulses 1, 2, 3, and 7) of the quenching analysis is shown. Measurements were performed on three different plants. B, Imaging of the second and seventh pulses of the quenching analysis on an exemplary plant during measuring days 0, 16, and 32 (top, middle, and bottom, respectively). The values of Φ_{NO} from 0 to 0.6 are mapped as a color gradient (from dark violet to light yellow, respectively). The color scale is shown on the right. C, Ternary plots of energy distribution in plants measured on days 0 and 32 (red and blue colors, respectively). The axes (sides of an equilateral triangle) represent Φ_{PSII}, Φ_{NPQ}, and Φ_{NO} parameters. The contours represent estimates of borders of regions encompassing 99.73%, 95.45%, 68.75%, and 20% of sample points. Traces of changing color (blue to red) represent changes in the average energy partitioning parameters through the whole assessed growth period.

performances at different photosynthetic induction stages. The extent of short-term light responses is different in old and young leaves, and the overall photosynthetic capacity of the plant's leaves changes with its age.

Statistical Analysis

The aim of this statistical analysis was to test if the leaf age and the plant age influence energy partitioning, both separately and in conjunction (for details, see Supplemental Mathematical Appendix S1). In our approach, we constructed a series of models. Each model links the expected energy partitioning to the values of the measured control variables, such as the pulse number u, the plant number p, the age of the rosette t_R, and the age of the leaf t_L. The models are represented schematically in Figure 7. There are three expected quantum yields $(\mu_{NPQ}, \mu_{PSII}, \mu_{NO})$, which we estimate based on the observed triplets of quantum yields $(\varphi^i_{NPQ}, \varphi^i_{PSII}, \varphi^i_{NO})$. If a simple linear regression was used to model each quantum yield separately, it could result in physically uninterpretable negative predictions. Also, in that case, the predictions probably would not sum to 1.

The Dirichlet regression offers a well-studied approach to analyze such data (for a self-contained introduction, see Supplemental Mathematical Appendix S1). In general, this approach postulates a linear relationship between the logarithms of the ratios μ_{NPQ}/μ_{NO} and μ_{PSII}/μ_{NO} and the control variable x_i, given by

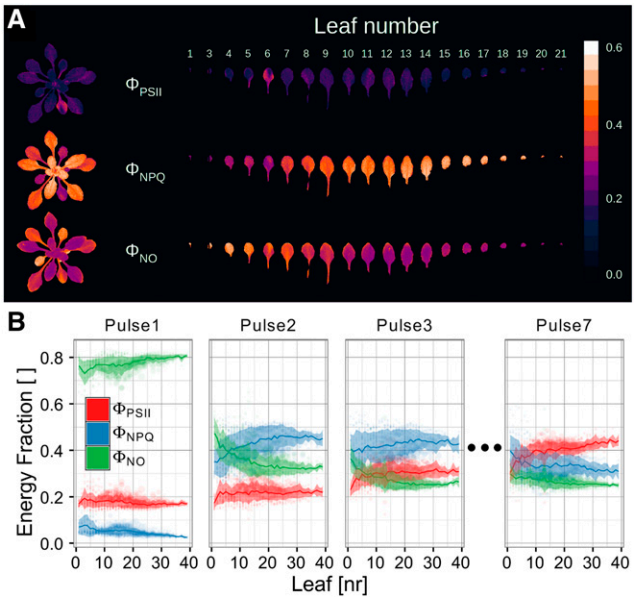

Figure 4. Changes in energy partitioning for different leaves, in order of appearance. A, Imaging of Φ_{PSII}, Φ_{NPQ}, and Φ_{NO} (top to bottom rows, respectively) on the rosette (20 d old) and on separate leaves from that rosette (left and right). As the leaf number is a value describing the order of appearance, a lower leaf number means an older leaf. Only the second pulse of the measurement is shown. The values of Φ_{NO} from 0 to 0.6 are mapped as a color gradient (from dark violet to light yellow). The color scale is shown on the right. B, Changes in Φ_{PSII}, Φ_{NPQ}, and Φ_{NO} (red, blue, and green color, respectively) plotted against the order of appearance of leaves. For readability, only pulses 1, 2, 3, and 7 are shown. For each measured leaf, the values of each quantum yield were averaged on the whole leaf area. Each separate estimate, from leaves of three different plants during 32 d of growth, is shown as a point with a radius scaled by the size of the leaf. Solid lines and their shadows correspond to the averaged quantum yields for leaves of a specific order of appearance and the SD.

$$log\frac{\mu_{NPQ}}{\mu_{NO}} = \beta_a^{NPQ} + \sum_i x_i A_{b,i}^{NPQ}$$

$$log\frac{\mu_{PSII}}{\mu_{NO}} = \beta_a^{PSII} + \sum_i x_i A_{b,i}^{PSII}$$

Above, $A_{b,i}^{NPQ}$ and $A_{b,i}^{PSII}$ denote the parameters measuring the strength of impact of a particular control, variable x_i. Figure 7 presents all considered forms of the above relationship. All models contain a constant term, denoted by appropriately superscripted β. The parameters can be interpreted as changes in the considered log ratios inflicted by a unit change in a particular control variable. The constant factors β represent the values of the logarithms of the ratios μ_{NPQ}/μ_{NO} and μ_{PSII}/μ_{NO} at the beginning of the measurements, when both the age of the rosette and the age of the leaf equal zero.

Models in Figure 7 are related to each other and designed to gradually deepen the form of dependence between the expected quantum yields and other data. To validate how complicated a model should get to best reflect reality, we performed a model selection procedure. Models were compared with two different quality metrics: the asymptotic likelihood ratio test and the average error on the validation sets in a k-fold cross-validation (Hastie et al., 2009; Wasserman, 2010).

The likelihood ratio test is a statistical method used to compare nested models. A simpler model is nested in a complex model if it can be obtained from the latter by imposing constraints on its parameters. For instance, model 1 is nested in model 2, because if all pulse-dependent average effects were the same (i.e. $\beta_{u_1} = \beta_{u_2} = \ldots = \beta_{u_7} = \beta$), then both models would be algebraically equivalent. Note that model 1 also is nested in all the other models and that model 4 is not nested in model 5, nor is the opposite true. As shown, the calculated P values are always below 2.2×10^{-16}, which is a powerful indication that more complex models fit the data better. In particular, the tests reject the null hypothesis at a significance level equal to 1‰. However, it is widely known that such results might be deceptive. Indeed, models with more covariates usually fit the data better, which does not mean that they can correctly predict outcomes better than simpler models on some other data sets. In other words, overfitted models generalize poorly. To minimize this risk, we tested all models in a k-fold cross-validation scheme. By the nature of cross-validation, the estimated parameters are random, because of the random division of the original data set into k parts. Even so, the SD values are orders of magnitude smaller than their average values, so we do not report them.

Finding Influential Parameters

The simplest considered model, model 1, treats energy partition as constant and independent of any considered control variables. Model 2 includes the effect of the pulse number on the response variables, leading to a significant improvement in both considered quality metrics. We observed a large drop in the average cross-validation error rate from 13.9% to 4.9% (Fig. 7). This means that model 2 predicts the data on average 2.8 times better than its predecessor. Also, the observed differences in log likelihoods (DLL) in this model were huge (29,083) compared with all other DLL values (all others were smaller than 4,000). This large difference is intuitive, as the average energy partitions differ from one pulse to another (Fig. 1). Model 1 simply does not have enough degrees of freedom to capture that trend.

To validate the impact of the phenotypic variation, we included the dependence of the average response on the plant number p in model 3. This model only slightly improved on its predecessor in terms of accuracy (DLL = 464), reducing the difference between average errors by one-tenth of 1% the point of the maximal error.

Carvalho et al. (2015) showed that plant age highly influences the photoprotective capacity of plants, so we

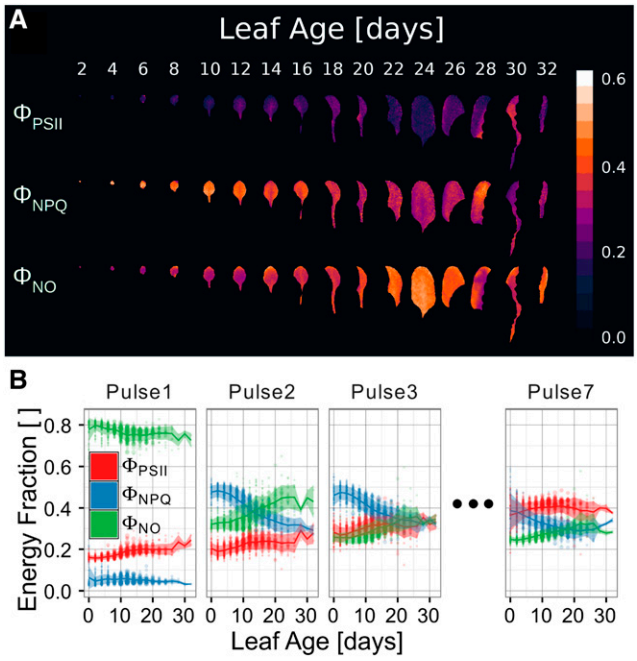

Figure 5. Changes in energy partitioning depending on the leaf age. A, Imaging of Φ_{PSII}, Φ_{NPQ}, and Φ_{NO} (top to bottom rows, respectively) of the same, eighth leaf during its 32 d of growth. Only the second pulse of the measurement is shown. Values are mapped to colors as seen on the scale on the right. B, Changes in the Φ_{PSII}, Φ_{NPQ}, and Φ_{NO} (red, blue, and green color, respectively) during quenching analysis are shown as a function of the leaf's age. For readability, only pulses 1, 2, 3, and 7 are plotted. For each measured leaf, the values for each quantum yield were averaged on the whole leaf area. Each separate estimate from leaves of three different plants, during 32 d of growth, is shown as a point with a radius scaled by the size of the leaf. The number of leaves shown for each age level is different, as all the leaves of a certain age are shown throughout the whole growth of three different plants. Solid lines and their shadows correspond to the averaged quantum yields for leaves at a specific age and the SD.

included the effect of the plant's age in model 4. We assumed the simplest linear form of dependence with plant age. Comparing model 4 with model 3, we conclude that plant age has a significant influence on the partition of energy, as DLL = 2,885 and the average error drops by more than 4 percentage points.

To validate if the leaf age effect could replace the plant age in explaining the above differences, we constructed model 5. This model also extends model 3. Both models were nested in a larger model 6, which incorporated both effects simultaneously. The comparison of the last four models leads to the conclusion that both time parameters must be considered jointly while studying their effect on the energy partitioning: DLL = 3,396 between model 6 and model 4 and DLL = 2,711 between model 6 and model 5, while the error drops in both cases by approximately half a percentage point of the maximal error.

Exploratory analysis underlined the importance of pulse number u on the quantum yields (Figs. 1 and 6). This motivated the construction of model 7, which adds pulse-specific effects on the leaf and plant age parameters. The increase in accuracy is small in absolute numbers: it makes on average 3‰ less error compared with model 7, with DLL = 2,308.

Finally, we built model 8 to study the nonlinearity in the time dependencies. The model adds quadratic terms for the plant and leaf age and an interaction term. It is a second-order Taylor expansion of the true regression function. The inclusion of the quadratic terms leads to further minor improvements, as DLL = 1,427 and the average error drops by roughly one-fifth of 1% of the maximal error.

We report the precise estimates of all the parameters of the final model 8 in Supplemental Mathematical Appendix S1 (Supplemental Tables S1–S3). With pulse number, the estimated parameters converge toward the steady-state values (Supplemental Fig. S4).

The distribution of errors of model 8 is elliptical (Supplemental Figs. S5 and S6), which is what one should expect from maximum likelihood estimators (Wasserman, 2010). The concentration of errors indicates that the chosen set of control variables explains well the studied phenomenon. Moreover, model 8 effectively removes the noise from the data (Supplemental Fig. S7).

To conclude, the above framework confirmed that the leaf and plant age are important factors that both influence the energy partitioning. The effects of these factors are different in the initial measurements and the steady-state values of the quenching analysis.

Long-Term High-Light Acclimation

As shown before in our exploratory and statistical analysis, energy partitioning between leaves differed mostly in NPQ-related parameters, which is relevant for their photoprotection. To check this, we subjected 5-week-old Arabidopsis plants grown previously under standard conditions (8 h per day of 200 μmol photons m^{-2} s^{-1}) to HL (1,800 μmol photons m^{-2} s^{-1}). As a measure of photoinhibition, we calculated the maximum quantum yield of PSII (F_V/F_M) before and after long-term HL treatment (2 d long). F_V/F_M describes the state of Φ_{PSII} when the plant is dark adapted and NPQ is inactivated (Butler and Kitajima, 1975; Kitajima and Butler, 1975). It shows the maximum fraction of absorbed energy that can be directed for photochemistry. F_V/F_M was measured every other day for a total of 8 d.

During long-term HL acclimation, most plants experienced an initial decrease in F_V/F_M followed by a return to the range of values observed at the onset (Fig. 8, top). An F_V/F_M decrease suggests more photodamage to PSII. To investigate the relationship between F_V/F_M and the leaf number, we performed the rosette decomposition as described earlier (Fig. 8, bottom). Older leaves were more prone to photodamage than younger ones, and the youngest leaves did not show any sign of photoinhibition.

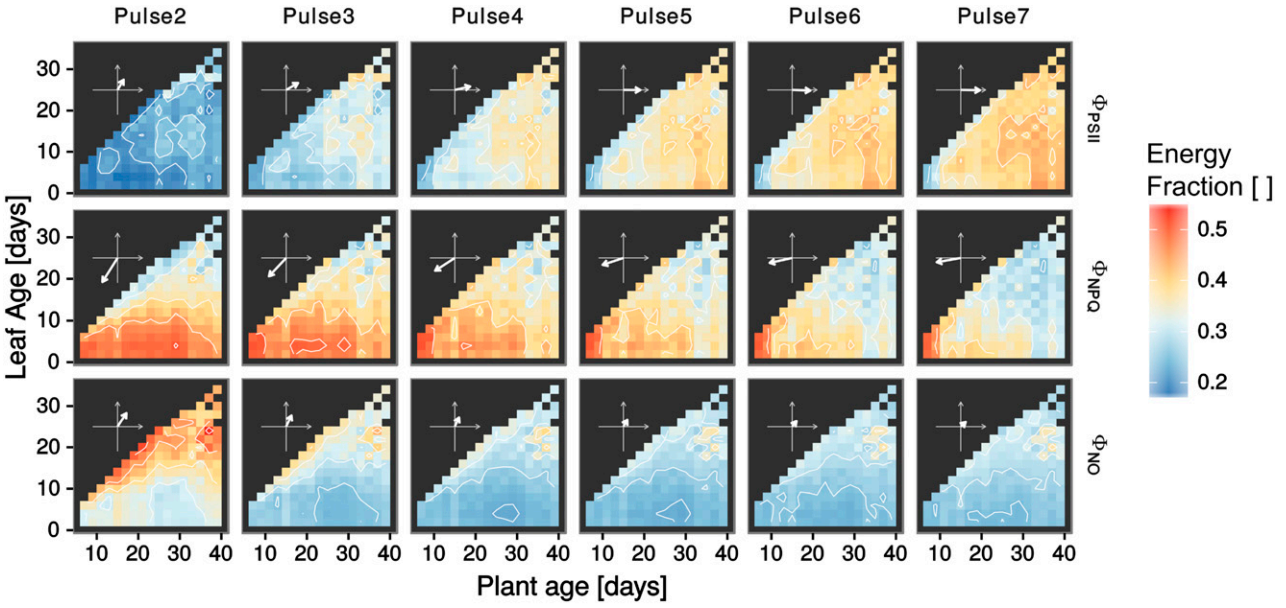

Figure 6. Combined effects of the age of the plant and its leaves on energy partitioning. Changes in Φ_{PSII}, Φ_{NPQ}, and Φ_{NO} (top to bottom rows, respectively) during quenching analysis are shown as a function of the age of the plant and the age of the leaves. The average values spanned between 20% and 50% of the total energy and are depicted as colors (blue, white, yellow, and red) in each pulse and quantum yield. In the corner of each image, the arrow represents the change due to the age of the plant and of the leaf (*x* and *y* axes). On the ordinate, the difference between the averaged values from all leaves of the oldest plants to all leaves of the youngest plants, and on the abscissa, the difference between the averaged values from the oldest or youngest leaves on plants of all ages, are shown. The arrow is a result of the combined effects of the full extent of the value change due to each variable.

Effect of the Light Intensity

The leaf distance from the light source could influence the measured energy partitioning, as this effect is equivalent to exposure to a different light intensity. To check this, we performed a quenching analysis on selected leaves from wild-type plants under three AL intensities (200, 600, and 1,000 μmol photons m^{-2} s^{-1}; Fig. 9A).

As expected, under HL, a smaller fraction of the absorbed energy was directed into photochemistry, while most of the energy was quenched through regulated NPQ. At the steady-state time point, this resulted in lower values of Φ_{PSII} and higher Φ_{NPQ}. The steady-state value of Φ_{PSII} was reached at the same time, independently of the light intensity. The initial Φ_{NPQ} rise was the same in all cases, but then, depending on the light intensity, it stabilized at the steady-state values or declined. This effect is due to the interplay between the buildup of the pH potential across the thylakoid membrane and the dissipation of it by ATP synthase (Schöttler et al., 2015). The Φ_{NO} kinetics and levels were not affected by the light intensity.

We could conclude that, in our previous experiments, differences in Φ_{NPQ} and Φ_{NO} observed especially at the early stage of the dark-to-light transition could not be attributed to the distance of the leaf from the light source. The changes observed in the steady-state levels (i.e. higher Φ_{PSII} and lower Φ_{NPQ} in older plants) might suggest that older plants are more efficient in using the intercepted light. When the plants get older, the rosette becomes slightly convex, and the plants could experience a slightly higher light intensity in the center. However, this would lead to a decreased Φ_{PSII} and an increased Φ_{NPQ}; instead, the opposite effect is observed.

DISCUSSION

In this work, we investigated the effect of the plant and leaf age on the full kinetics of energy partitioning during the dark-to-light transition. We observed heterogeneity between the leaves of the rosette in terms of both photosynthetic and photoprotective capacity. The effects of the age of the plant and its leaves intertwine and must be considered jointly in order to properly address their precise influence on energy partitioning.

Plant Age Effect

The effect of the plant's age was mostly observed at steady-state values and corresponds to an increased level of Φ_{PSII} and decreased Φ_{NPQ} in older plants (Fig. 6). We suggest that the observed increase of PSII efficiency in older plants in nonstress conditions might come from the reduced limitation on the LEF due to an increased accumulation of Rubisco (Johansson et al., 2004). The decrease in NPQ would then be a secondary effect of the increase of CO_2 assimilation capacity. These suggestions can be supported by the opposite trend

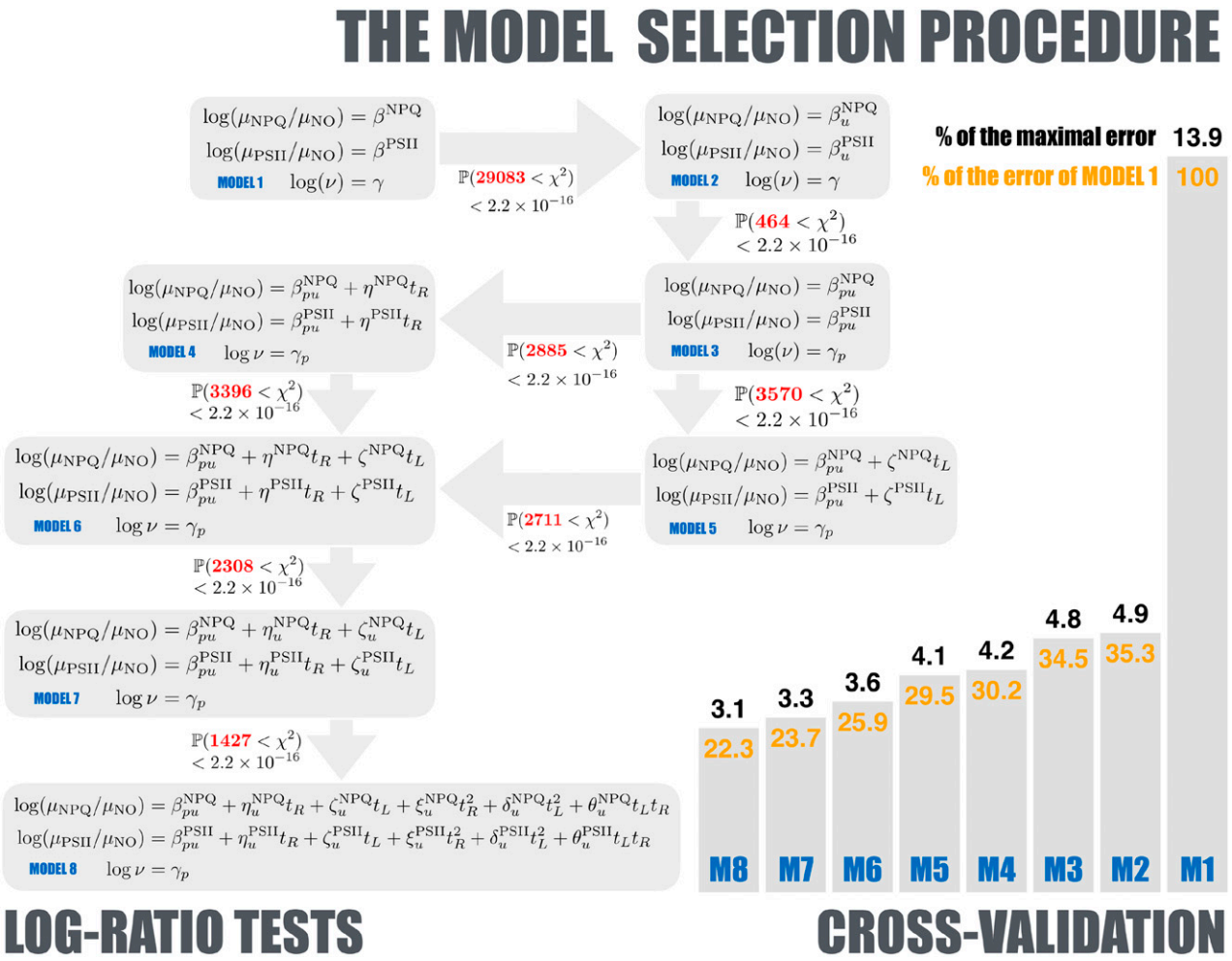

Figure 7. The model selection procedure. Models are represented as a chain of rectangular gray areas on the left. Each model consists of a set of exactly three equations relating expected energy fractions (μ_{NPQ}, μ_{PSII}, μ_{NO}) and the precision parameter to the control variables (for details, see Supplemental Mathematical Appendix S1). Presented models are partially ordered by their complexity, from the most simple one (top left corner) to the most complicated one (bottom left corner). The coefficients of the age of the rosette t_R parameters are denoted by η, the coefficients of its square t_R^2 are denoted by ξ, the coefficients of the age of leaf t_L are denoted by ζ, and the coefficients of its square are denoted by δ. Finally, the coefficient of the mixed effect parameter $t_L t_R$ is denoted by θ. We denote different constants by additional subscripts. Some models assume that different constants can be fitted for different pulse numbers u. Additionally, if the constants depend on the plant number, p, we denote the full dependence by β_{pu}. Gray arrows indicate the direction of the growing complexity. Included parameters are described in "Results." Next to the arrows, we plot the computed values of the log ratio test statistic $\chi^2_{computed}$ (boldface red numbers). The P values are shown below. The bar chart on the right presents the cross-validation results. The bars are related to models as indicated by their blue tags at the bottom of each bar. Bar heights correspond to the different predicative capabilities of the models: these can be expressed in absolute terms, as a percentage of the maximal achievable error (number in black above each bar), or in relative terms, as a percentage of the error of the first model (number in light orange below the top edge of each bar).

(decreased Φ_{PSII} and increased Φ_{NPQ}) observed in plants subjected to HL (Fig. 9), low temperature (10°C; Hendrickson et al., 2004), and CO_2 limitation (Kramer et al., 2004). In all three cases, the changes in energy partitioning can be attributed to a limitation of the LEF. When light is absorbed in excess (i.e. under HL and CO_2 limitation), the photosynthetic performance is limited by the electron transfer and the CO_2 assimilation capacity (Genty et al., 1989). Under low temperature, the origin of the phenomenon is due to the thermal slowdown of the diffusion of the electron carriers and enzymes responsible for CO_2 assimilation.

Leaf Age Effect on Short-Term Responses

We observed changes in energy partitioning related to leaf age mostly in the early stages of the dark-to-light transition (Figs. 5 and 6). While the leaf aged, the energy previously allocated to Φ_{NPQ} was redirected gradually

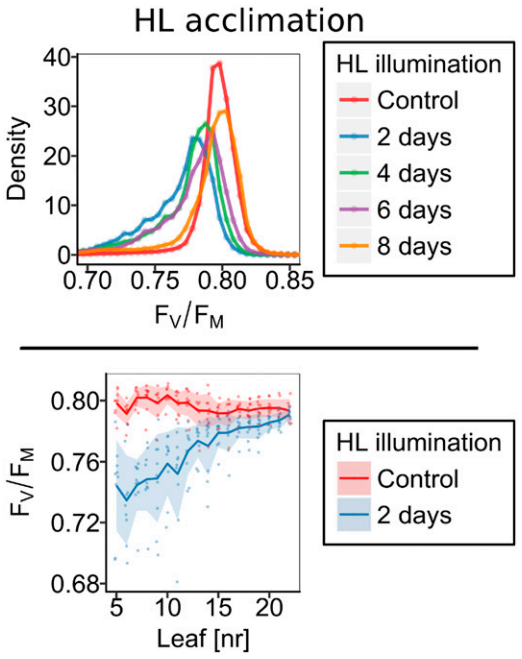

Figure 8. Changes in F_V/F_M during long-term HL acclimation. Top, Exemplary histogram of the F_V/F_M values during 8 d of HL acclimation (red, blue, green, purple, and orange) resulting from fluorescence imaging of a selected plant. Bottom, Values of F_V/F_M as a function of leaf number before (Control) and after 2 d of HL illumination (red and blue, respectively). Points represent averaged values from each leaf from 10 different plants. Average and SD from all plants, for a selected leaf number, are drawn as a line and a shadow, respectively.

to Φ_{NO}. This could be a characteristic of younger leaves decreasing photoinhibition during changes in light intensities (Li et al., 2002), as they respond more dynamically (i.e. by triggering NPQ faster) than older leaves.

The effect of leaf age became insignificant while reaching steady-state levels. This is not unexpected, as during leaf growth the photosynthetic apparatus, after being properly assembled, does not change much (Nath et al., 2013). According to our findings, the Φ_{PSII} did not change, and the decrease in assimilation rate with the age of the leaf observed by Stessman et al. (2002) should be explained by other factors than the alteration of LEF capacity.

Leaf Age Effect on Long-Term Acclimation

Under long-term (hours to days) HL, the leaf can acclimate through molecular (Anderson et al., 1995; Ballottari et al., 2007; Kouřil et al., 2013), anatomical, and physiological changes (Oguchi et al., 2003). To increase photosynthetic capacity, the thickening of the mesophyll layer to increase the gas-exchange area and the increase in Rubisco activity are indispensable. However, those changes happen only when the leaf is young enough (Sims and Pearcy, 1992). As there was little and indirect information about the photoprotective capacity as a function of leaf age in Arabidopsis, we tested the capacity of all visible leaves on a rosette for long-term HL acclimation (Fig. 8). The results indicated that younger leaves were better photoprotected under continuous excessive light intensity than the older ones (they exhibited a smaller drop in F_V/F_M).

Additionally, there may be other photoprotective pathways that are not detectable with PAM fluorescence measurements that can increase the photoprotective capacity of younger leaves. For example, it was shown that younger leaves have a higher capacity to accumulate ascorbate peroxidase and superoxide dismutase (Sperdouli and Moustakas, 2012; Moustaka et al., 2015). Both enzymes are part of the reactive oxygen species scavenging system, a separate photoprotective mechanism not related to NPQ. This scavenging system may be responsible for the increased plasticity of young leaves during a broad range of stress responses. A higher anabolic activity in young, still expanding leaves (Vanhaeren et al., 2015) could lead to the modification of the leaf anatomy and a faster synthesis and degradation of cellular components (redesign of the photosynthetic apparatus) needed for effective acclimation (Anderson et al., 1995; Ballottari et al., 2007; Kouřil et al., 2013). An enhanced repair cycle of PSII in younger leaves could cause a similar effect (Aro et al., 2005). Its activity changes during HL acclimation; however, it is not known if it differs between leaves of different ages. That any of these mechanisms

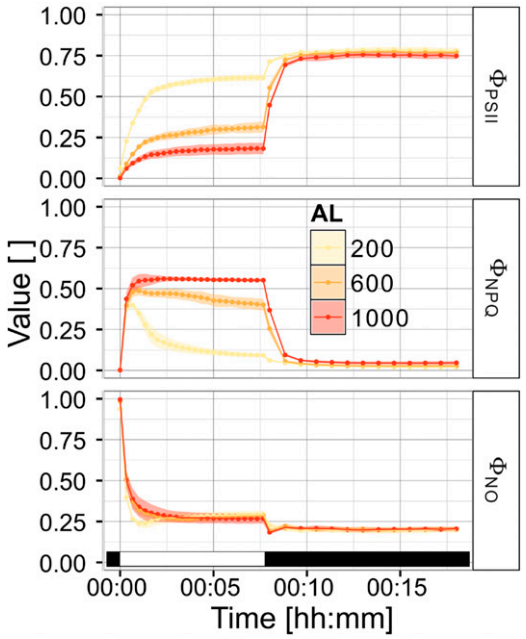

Figure 9. Energy partitioning under different AL. Energy distribution in PSII, Φ_{PSII}, Φ_{NPQ}, and Φ_{NO} (top, middle, and bottom, respectively), is shown for wild-type plants illuminated for 8 min with 200, 600, and 1,000 μmol photons m^{-2} s^{-1} (yellow, orange, and brown traces, respectively; $n = 3$). Periods of illumination and darkness are indicated as white and black bars at bottom.

are responsible for the increased photoprotection is still not clear, and further investigation is needed.

In conclusion, we suggest that the changes we observed in energy partitioning due to leaf age are an adaptation to dynamic changes in light conditions. Better acclimation of younger leaves to high continuous light is probably not due to NPQ-related mechanisms but to a higher plasticity of the young leaves that can quickly redesign their leaf anatomy and photosynthetic apparatus, optimizing it to the new light conditions.

Potential Applications and Future Perspectives

Leaf and plant age are important parameters to be taken into consideration, especially in photosynthetic phenotyping during genetic and stress-related studies. Both may highly influence the assessment of photosynthetic and/or photoprotective capacity. Taking leaf and plant age into account will lead to a more accurate and representative characterization of plants.

First, our study underlines the importance of leaf age in any studies of NPQ induction in folio. A simple choice of a leaf on a rosette can lead to a range of different rates of NPQ induction. An arbitrary choice of a leaf may not reflect the whole range of responses that one can observe on the plant.

Second, steady-state PAM fluorometry is commonly used to assess the photosynthetic and photoprotective capacities of the plant. As the plant's age can influence both, it must become a crucial parameter to be considered. However, there are situations in which even considering plant age might not be enough. In some cases, the growth and development of the plant might be delayed, due to genetic or environmental factors (Nord and Lynch, 2008). Then, the choice of a representative time point is not possible and the only solution is to characterize the plant throughout the whole growth period.

Finally, our modeling approach significantly simplifies the description of the experiments by massively reducing the dimensionality of the data: 115 estimated parameters in the last model 8 instead of around 12,000 real numbers. Different data sets can be compared using the estimated coefficients.

CONCLUSION

In this study, we show that the ages of the leaf and of the plant have a combined effect on the photosynthetic parameters at various stages of the chlorophyll fluorescence quenching analysis. An increase in the photosynthetic performance at steady-state levels is observed when the plant gets older. In terms of short-term responses, the age of the leaf most significantly affects the early kinetics of the dark-to-light transition (i.e. the fast response to changes in light conditions). Younger leaves trigger NPQ faster. In terms of HL acclimation, we show that old leaves acclimate less well than young leaves to continuous light stress. Our results indicate that the ages of the plant and of its leaves become important parameters that should be taken into account when choosing both the time of measurements and the selection of leaves, particularly when comparing the photosynthetic performances of wild-type and mutant plants in genetic and stress-related studies.

MATERIALS AND METHODS

Plant Material

Developmental Experiment

The seeds of Arabidopsis (*Arabidopsis thaliana*) ecotype Columbia-0 were germinated in a nursery built as described by Noren et al. (2004; Supplemental Fig. S1), with some modifications. The seeds were first sterilized (5 min in a 70% ethanol solution followed by 2 min in a 0.5% SDS solution). Then, they were planted on top of 100-μL pipette tips, with melted ends, and filled with a Murashige and Skoog agar solution (Supplemental Fig. S1A). The seeds were then vernalized (darkness and 4°C for 3 d). From the cold room, for the next 2 weeks, the Arabidopsis nursery was transferred to the growth chamber (AR-36L; Plant Climatics Percival) with controlled humidity (75%), photoperiod (8-h day/16-h night), temperature (21°C), and light intensity (100 μmol photons m^{-2} s^{-1}). Then, they were transferred to the hydroponic setup and grown there for 6 weeks (Supplemental Fig. S1B). The hydroponic setup consisted of non-transparent plastic containers filled with a nutrient solution of pH 5.8 to 6 that was constantly aerated with an external air pump. Plants in pipette tips were inserted in 8- × 8-cm coated black, polystyrene plates that floated on top of the liquid medium.

Long-Term HL Acclimation

For the experiment testing long-term HL acclimatory capacity, Arabidopsis (ecotype Columbia-0) wild-type seeds were sown on Murashige and Skoog medium agar plates. The seeds were vernalized (darkness and 4°C for 3 d) and transferred to the growth chamber (AR-36L; Plant Climatics Percival) and kept under standard conditions (70% relative humidity, 21°C, photoperiod of 8/16 h, and 200 μmol photons m^{-2} s^{-1}). After 5 to 7 d, the seedlings were transplanted to final pots. As a control, plants were grown for 6 weeks under standard conditions. For the HL treatment, the plants were grown initially together with the control. After 5 weeks, a batch of plants was transferred and grown for an additional 8 d under 1,800 μmol photons m^{-2} s^{-1} (FytoScope FS 3400; Photon Systems Instruments).

Semiautomatic Rosette Image Disassembly

For image analysis, we adapted the plant and leaf segmentation introduced by Scharr et al. (2016). During quenching analysis, the signal-to-noise ratio was lowest in F_M images (Supplemental Fig. S3A). We then used F_M images to set the threshold for the background exclusion and create foreground, binarized masks. Afterward, we created Euclidean distance maps with leaf centers as local peaks. The leaf centers also were used as watershed seeds (Belaid and Mourou, 2009). As the plants got older, we faced an increasing number of problems related to misidentification of the leaf centers. The leaves, imaged from above, unavoidably started to overlap during some phase of their growth, and clusters of leaves could be erroneously mistaken for one leaf. Thus, we included a manual correction step to properly identify leaves and their order of emergence.

Fluorescence Measurements

Whole-Plant Imaging

The imaging during active fluorescence measurements was performed using an Open FluorCAM FC 800-O/1010 (Photon-System Instruments). Measurements were performed each second day after the start of the experiment at room temperature and in ambient atmosphere. Spatial resolution was established prior to each measurement. On the image, each pixel corresponded to an area

between 0.02 and 0.05 mm^2. As AL and during SPs, two white LED panels were used, and as measuring light (ML), two red (630-nm) LED panels were used. During each SP, we collected 10 frames, which afterward were averaged. The quenching analysis protocol created by the protocol wizard (FluorCAM 7 software) was modified to achieve lower noise throughout the measurement. After a night of dark adaptation, F_0 was measured, followed by SP (1 s of 3,000 μmol photons m^{-2} s^{-1}) to measure F_M. During the dark-to-light transition (5 min of 1,000 μmol photons m^{-2} s^{-1} AL), an SP of 1 s was given to determine F_M', every 41 s over seven repetitions. Prior to each SP, F_t was measured using only ML on top of AL. After the light was switched off, in the relaxation phase (light-to-dark transition), we measured F_M and F_t values three times during the following 3 min. By using the measured parameters, F_V/F_M, Φ_{PSII}, Φ_{NPQ}, and Φ_{NO} were calculated based on Butler and Kitajima (1975), Genty et al. (1989), and Klughammer and Schreiber (2008) as follows:

$$F_V/F_M = \frac{F_M - F_0}{F_M}$$

$$\Phi_{PSII} = \frac{F_m' - F_t}{F_m'}$$

$$\Phi_{NPQ} = \frac{F_t}{F_m'} - \frac{F_t}{F_M}$$

$$\Phi_{NO} = \frac{F_t}{F_M}$$

Single Leaf Measurement

To perform a standard quenching analysis, a DualPAM-100 fluorometer (Walz) was used. The measurements were performed on fully extended 8- to 10-d-old leaves from 4-week-old plants grown under standard conditions. Intact leaves were measured at room temperature and in ambient atmosphere. SP was a red light pulse (630 nm), 500 ms long, of 5,000 μmol photons m^{-2} s^{-1}. ML intensity was 3 μmol photons m^{-2} s^{-1}. To follow the dark-to-light transition, plants were illuminated for 8 min with a selected AL intensity (200, 600, or 1,000 μmol photons m^{-2} s^{-1}). Every 20 s, the measured leaf was subjected to a 5-s far-red preillumination and an SP to measure F_M. A light-to-dark transition was then registered after switching off the AL, where an SP was applied every 50 s for the next 10 min to measure F_t and F_M'. The parameters were calculated as described above.

Statistical Analysis

Data exploration and statistical analysis were performed using Python and R. The plots were created using the ggplot2 (Wickham, 2009) and ggtern (Hamilton, 2016) R project packages, ImageJ 2.0 (Schindelin et al., 2012), and GIMP. Data were prepared using the packages plyr (Wickham, 2011), dplyr (Wickham and Francois, 2016), and tidyr (Wickham, 2016).

The statistical analysis involved the fitting of several nested Dirichlet regression models (Aitchison, 1986). Nested Dirichlet regression models provide a theoretical framework for the study of the dependence between observed percentage changes in energy partitioning and the levels of other variables describing the system.

Models were compared with two different quality metrics: the asymptotic likelihood ratio test and the average error on the validation sets in a k-fold cross-validation (Hastie et al., 2009; Wasserman, 2010).

The null hypothesis in the likelihood ratio test assumes no significant differences between the simple and the unconstrained model. We report the DLL as dimensionless numbers. Bigger values indicate that the complex model explains the observed data better than the simpler one. The null hypothesis is rejected if the probability of the critical set of these statistics is below a given significance level α.

To minimize the risk of overfitting, we tested all models in a k-fold cross-validation scheme. The data set was first divided at random into k approximately equal subsets. Then, all subsets but one were merged, and the model was estimated on the resulting bigger set and then tested on the left-out validation set. We fitted the models iteratively k times and tested them on the validation sets. After each fit, we compared the models' predictions with true values using the Euclidean distance. The obtained errors are positive and limited from above by $\sqrt{2}$ – the maximal distance between the real partition and its prediction. The errors were averaged over all results in a given validation set and over all validations sets and then normalized to the maximum obtainable error:

$$Averageerror = \frac{1}{k\sqrt{2}} \sum_{j=1}^{k} \frac{1}{n_j} \sum_{i=1}^{n_j} \sqrt{\left(\phi^i_{NPQ} - \hat{\phi}^i_{NPQ}\right)^2 + \left(\phi^i_{PSII} - \hat{\phi}^i_{PSII}\right)^2 + \left(\phi^i_{NO} - \hat{\phi}^i_{NO}\right)^2}$$

Above, n_j is the number of elements in the j-th validation set, $(\phi^i_{NPQ}, \phi^i_{PSII}, \phi^i_{NO})$ are the observed quantum yields, and $(\hat{\phi}^i_{NPQ}, \hat{\phi}^i_{PSII}, \hat{\phi}^i_{NO})$ are the predicted quantum yields obtained by the model under consideration. The resulting average error was used as a quality metric of a particular model in the model selection procedure.

A detailed description of the statistical work flow is presented in Supplemental Mathematical Appendix S1. All models were fitted using the R package DirichletReg (Maier, 2014, 2015).

Supplemental Data

The following supplemental materials are available.

Supplemental Figure S1. Nursery and hydroponic setup.

Supplemental Figure S2. Exemplary fluorescence trace.

Supplemental Figure S3. Image-analysis pipeline for rosette disassembly.

Supplemental Figure S4. Estimated coefficients of model 8.

Supplemental Figure S5. Model 8 predictions versus the actual measurements for different combinations of pulse numbers and plants.

Supplemental Figure S6. Distribution of errors of model 8 for different combinations of pulse numbers and plants.

Supplemental Figure S7. Levels of energy partitions as a function of plant and leaf age.

Supplemental Table S1. Results of estimating the parameters of model 8.

Supplemental Table S2. Results of estimating the parameters of model 8 (continued).

Supplemental Table S3. Results of estimating the parameters of model 8 (continued).

Supplemental Table S4. Conditional numbers of estimated hessians of all considered models.

Supplemental Mathematical Appendix S1. Statistical model formulation and detailed statistical analysis.

ACKNOWLEDGMENTS

We thank Rikard Fristedt for help with setting up the hydroponic setup and Bart van Oort, Gert Schansker, Peppijn van Oort, and Michael Gruber for helpful discussion.

Received July 6, 2017; accepted October 6, 2017; published October 10, 2017.

LITERATURE CITED

Aitchison J (1986) The Statistical Analysis of Compositional Data. Chapman & Hall, London

Anderson JM, Chow WS, Park YI (1995) The grand design of photosynthesis: acclimation of the photosynthetic apparatus to environmental cues. Photosynth Res **46:** 129–139

Aro EM, Suorsa M, Rokka A, Allahverdiyeva Y, Paakkarinen V, Saleem A, Battchikova N, Rintamäki E (2005) Dynamics of photosystem II: a proteomic approach to thylakoid protein complexes. J Exp Bot **56:** 347–356

Ballottari M, Dall'Osto L, Morosinotto T, Bassi R (2007) Contrasting behavior of higher plant photosystem I and II antenna systems during acclimation. J Biol Chem **282:** 8947–8958

Belaid LJ, Mourou W (2009) Image segmentation: a watershed transformation algorithm. Image Anal Stereol **28:** 93–102

Bresson J, Vasseur F, Dauzat M, Koch G, Granier C, Vile D (2015) Quantifying spatial heterogeneity of chlorophyll fluorescence during plant growth and in response to water stress. Plant Methods **11:** 23

Brouwer B, Ziolkowska A, Bagard M, Keech O, Gardeström P (2012) The impact of light intensity on shade-induced leaf senescence. Plant Cell Environ **35:** 1084–1098

Butler WL, Kitajima M (1975) Fluorescence quenching in photosystem II of chloroplasts. Biochim Biophys Acta **376:** 116–125

Cailly AL, Rizza F, Genty B, Harbinson J (1996) Fate of excitation at PS II in leaves: the non-photochemical side. Plant Physiol Biochem p 86

Carmo-Silva AE, Salvucci ME (2013) The regulatory properties of Rubisco activase differ among species and affect photosynthetic induction during light transitions. Plant Physiol **161:** 1645–1655

Carvalho FEL, Ware MA, Ruban AV (2015) Quantifying the dynamics of light tolerance in Arabidopsis plants during ontogenesis. Plant Cell Environ **38:** 2603–2617

Cheeseman JM (1991) PATCHY: simulating and visualizing the effects of stomatal patchiness on photosynthetic CO_2 exchange studies. Plant Cell Environ **14:** 593–599

Demmig-Adams B (1990) Carotenoids and photoprotection in plants: A role for the xanthophyll zeaxanthin. Biochim Biophys Acta **1020:** 1–24

Demmig-Adams B, Adams WW III, Barker DH, Logan BA, Bowling DR, Verhoeven AS (1996) Using chlorophyll fluorescence to assess the fraction of absorbed light allocated to thermal dissipation of excess excitation. Physiol Plant **98:** 253–264

Flood PJ, Kruijer W, Schnabel SK, van der Schoor R, Jalink H, Snel JFH, Harbinson J, Aarts MGM (2016) Phenomics for photosynthesis, growth and reflectance in *Arabidopsis thaliana* reveals circadian and long-term fluctuations in heritability. Plant Methods **12:** 14

Genty B, Briantais JM, Baker NR (1989) The relationship between the quantum yield of photosynthetic electron transport and quenching of chlorophyll fluorescence. Biochim Biophys Acta **990:** 87–92

Genty B, Harbinson J, Cailly AL, Rizza F (1996) Fate of excitation at PS II in leaves: the non-photochemical side. The Third BBSRC Robert Hill Symposium on Photosynthesis, March 31 to April 3, 1996, University of Sheffield, Sheffield, UK, Abstract no. P28

Ghosh S, Mahoney SR, Penterman JN, Peirson D, Dumbroff EB (2001) Ultrastructural and biochemical changes in chloroplasts during *Brassica napus* senescence. Plant Physiol Biochem **39:** 777–784

Hamilton N (2016) ggtern: an extension to "ggplot2", for the creation of ternary diagrams. https://CRAN.R-project.org/package=ggtern

Hastie TJ, Tibshirani RJ, Friedman JH (2009) The Elements of Statistical Learning: Data Mining, Inference, and Prediction. Springer, New York

Hendrickson L, Furbank RT, Chow WS (2004) A simple alternative approach to assessing the fate of absorbed light energy using chlorophyll fluorescence. Photosynth Res **82:** 73–81

Hikosaka K, Terashima I, Katoh S (1994) Effects of leaf age, nitrogen nutrition and photon flux density on the distribution of nitrogen among leaves of a vine (*Ipomoea tricolor* Cav.) grown horizontally to avoid mutual shading of leaves. Oecologia **97:** 451–457

Hirose T, Werger MJA (1987a) Maximizing daily canopy photosynthesis with respect to the leaf nitrogen allocation pattern in the canopy. Oecologia **72:** 520–526

Hirose T, Werger MJA (1987b) Nitrogen use efficiency in instantaneous and daily photosynthesis of leaves in the canopy of a *Solidago altissima* stand. Physiol Plant **70:** 215–222

Jiang CZ, Rodermel SR (1995) Regulation of photosynthesis during leaf development in RbcS antisense DNA mutants of tobacco. Plant Physiol **107:** 215–224

Jiang CZ, Rodermel SR, Shibles RM (1993) Photosynthesis, Rubisco activity and amount, and their regulation by transcription in senescing soybean leaves. Plant Physiol **101:** 105–112

Johansson E, Olsson O, Nyström T (2004) Progression and specificity of protein oxidation in the life cycle of Arabidopsis thaliana. J Biol Chem **279:** 22204–22208

Kerstetter RA, Poethig RS (1998) The specification of leaf identity during shoot development. Annu Rev Cell Dev Biol **14:** 373–398

Kitajima M, Butler WL (1975) Quenching of chlorophyll fluorescence and primary photochemistry in chloroplasts by dibromothymoquinone. Biochim Biophys Acta **376:** 105–115

Klughammer C, Schreiber U (2008) Complementary PS II quantum yields calculated from simple fluorescence parameters measured by PAM fluorometry and the saturation pulse method. PAM Appl Notes **1:** 27–35

Kono M, Terashima I (2014) Long-term and short-term responses of the photosynthetic electron transport to fluctuating light. J Photochem Photobiol B **137:** 89–99

Kouřil R, Wientjes E, Bultema JB, Croce R, Boekema EJ (2013) High-light vs. low-light: effect of light acclimation on photosystem II composition and organization in Arabidopsis thaliana. Biochim Biophys Acta **1827:** 411–419

Kramer DM, Johnson G, Kiirats O, Edwards GE (2004) New fluorescence parameters for the determination of Q_A redox state and excitation energy fluxes. Photosynth Res **79:** 209–218

Lazár D (2015) Parameters of photosynthetic energy partitioning. J Plant Physiol **175:** 131–147

Li XP, Björkman O, Shih C, Grossman AR, Rosenquist M, Jansson S, Niyogi KK (2000) A pigment-binding protein essential for regulation of photosynthetic light harvesting. Nature **403:** 391–395

Li XP, Muller-Moule P, Gilmore AM, Niyogi KK (2002) PsbS-dependent enhancement of feedback de-excitation protects photosystem II from photoinhibition. Proc Natl Acad Sci USA **99:** 15222–15227

Maier MJ (2014) DirichletReg: Dirichlet regression for compositional data in R. http://epub.wu.ac.at/id/eprint/4077

Maier MJ (2015) DirichletReg: Dirichlet regression in R. http://CRAN.R-project.org/package=DirichletReg

Makino A, Mae T, Ohira K (1983) Photosynthesis and ribulose 1,5-bisphosphate carboxylase in rice leaves: changes in photosynthesis and enzymes involved in carbon assimilation from leaf development through senescence. Plant Physiol **73:** 1002–1007

Martínez-Peñalver A, Graña E, Reigosa MJ, Sánchez-Moreiras AM (2012) The early response of *Arabidopsis thaliana* to cadmium- and copper-induced stress. Environ Exp Bot **78:** 1–9

Miller A, Schlagnhaufer C, Spalding M, Rodermel S (2000) Carbohydrate regulation of leaf development: prolongation of leaf senescence in Rubisco antisense mutants of tobacco. Photosynth Res **63:** 1–8

Miller A, Tsai CH, Hemphill D, Endres M, Rodermel S, Spalding M (1997) Elevated CO_2 effects during leaf ontogeny (a new perspective on acclimation). Plant Physiol **115:** 1195–1200

Mohapatra PK, Joshi P, Ramaswamy NK, Raval MK, Biswal UC, Biswal B (2013) Damage of photosynthetic apparatus in the senescing basal leaf of *Arabidopsis thaliana*: a plausible mechanism of inactivation of reaction center II. Plant Physiol Biochem **62:** 116–121

Morison JIL, Lawson T (2007) Does lateral gas diffusion in leaves matter? Plant Cell Environ **30:** 1072–1085

Mott KA (2009) Opinion: stomatal responses to light and CO_2 depend on the mesophyll. Plant Cell Environ **32:** 1479–1486

Moustaka J, Tanou G, Adamakis ID, Eleftheriou EP, Moustakas M (2015) Leaf age-dependent photoprotective and antioxidative response mechanisms to paraquat-induced oxidative stress in *Arabidopsis thaliana*. Int J Mol Sci **16:** 13989–14006

Mulisch M, Krupinska K (2013) Ultrastructural analyses of senescence associated dismantling of chloroplasts revisited. Adv Photosynth Respir **36:** 307–335

Nath K, Phee BK, Jeong S, Lee SY, Tateno Y, Allakhverdiev SI, Lee CH, Nam HG (2013) Age-dependent changes in the functions and compositions of photosynthetic complexes in the thylakoid membranes of *Arabidopsis thaliana*. Photosynth Res **117:** 547–556

Nord EA, Lynch JP (2008) Delayed reproduction in Arabidopsis thaliana improves fitness in soil with suboptimal phosphorus availability. Plant Cell Environ **31:** 1432–1441

Noren H, Per S, Andersson B (2004) A convenient and versatile hydroponic cultivation system for *Arabidopsis thaliana*. Physiol Plant **121:** 343–348

Oguchi R, Hikosaka K, Hirose T (2003) Does the photosynthetic light-acclimation need change in leaf anatomy? Plant Cell Environ **26:** 505–512

Pfündel EE, Klughammer C, Meister A, Cerovic ZG (2013) Deriving fluorometer-specific values of relative PSI fluorescence intensity from quenching of F0 fluorescence in leaves of *Arabidopsis thaliana* and *Zea mays*. Photosynth Res **114:** 189–206

Quick WP, Stitt M (1989) An examination of factors contributing to non-photochemical quenching of chlorophyll fluorescence in barley leaves. Biochim Biophys Acta **977:** 287–296

Scharr H, Minervini M, French AP, Klukas C, Kramer DM, Liu X, Luengo I, Pape JM, Polder G, Vukadinovic D, et al (2016) Leaf segmentation in plant phenotyping: a collation study. Mach Vis Appl **27:** 585–606

Schindelin J, Arganda-Carreras I, Frise E, Kaynig V, Longair M, Pietzsch T, Preibisch S, Rueden C, Saalfeld S, Schmid B, et al (2012) Fiji: an open-source platform for biological-image analysis. Nat Methods **9:** 676–682

Schöttler MA, Tóth SZ, Boulouis A, Kahlau S (2015) Photosynthetic complex stoichiometry dynamics in higher plants: biogenesis, function, and turnover of ATP synthase and the cytochrome b_6f complex. J Exp Bot **66:** 2373–2400

Schreiber U, Klughammer C (2008) Non-photochemical fluorescence quenching and quantum yields in PS I and PS II: analysis of heat-induced limitations using Maxi-Imaging-PAM and Dual-PAM-100. PAM Appl Notes **1:** 15–18

Sims DA, Pearcy RW (1992) Response of leaf anatomy and photosynthetic capacity in *Alocasia macrorrhiza* (Araceae) to a transfer from low to high light. Am J Bot **79:** 449–455

Sperdouli I, Moustakas M (2012) Differential response of photosystem II photochemistry in young and mature leaves of *Arabidopsis thaliana* to the onset of drought stress. Acta Physiol Plant **34:** 1267–1276

Spreitzer RJ, Salvucci ME (2002) Rubisco: structure, regulatory interactions, and possibilities for a better enzyme. Annu Rev Plant Biol **53:** 449–475

Stessman D, Miller A, Spalding M, Rodermel S (2002) Regulation of photosynthesis during Arabidopsis leaf development in continuous light. Photosynth Res **72:** 27–37

Terashima I (1992) Anatomy of non-uniform leaf photosynthesis. Photosynth Res **31:** 195–212

Tikhonov AN (2015) Induction events and short-term regulation of electron transport in chloroplasts: an overview. Photosynth Res **125:** 65–94

Tsukaya H (2013) Leaf development. The Arabidopsis Book **11:** e0163, doi/10.1199/tab.0163

Vanhaeren H, Gonzalez N, Inzé D (2015) A journey through a leaf: phenomics analysis of leaf growth in Arabidopsis thaliana. The Arabidopsis Book **13:** e0181, doi/10.1199/tab.0181

Wada S, Ishida H, Izumi M, Yoshimoto K, Ohsumi Y, Mae T, Makino A (2009) Autophagy plays a role in chloroplast degradation during senescence in individually darkened leaves. Plant Physiol **149:** 885–893

Wasserman L (2010) All of Statistics: A Concise Course in Statistical Inference. Springer Publishing, New York

Wickham H (2009) ggplot2: Elegant Graphics for Data Analysis. Springer-Verlag, New York

Wickham H (2011) The split-apply-combine strategy for data analysis. J Stat Softw **40:** 1–29

Wickham H (2016) tidyr: easily tidy data with 'spread()' and 'gather()' functions. https://cran.r-project.org/package=tidyr

Wickham H, Francois R (2016) dplyr: a grammar of data manipulation. https://cran.r-project.org/package=dplyr

Wingler A, Marès M, Pourtau N (2004) Spatial patterns and metabolic regulation of photosynthetic parameters during leaf senescence. New Phytol **161:** 781–789